



Background Flow Model of Hall Thruster Neutral Ingestion

Jason D. Frieman,* Thomas M. Liu,† and Mitchell L. R. Walker‡
Georgia Institute of Technology, Atlanta, Georgia 30332

DOI: 10.2514/1.B36269

The particle-based coupling between background gas flows in vacuum test facilities and neutral ingestion into Hall effect thrusters is investigated. An analytical model of the facility background flow environment is developed to accommodate facilities with different geometries and pump placements, as well as compute the ingested flow rate of background neutrals into a given Hall effect thruster. The ingested flow rates computed by the model are shown to predict previous empirical datasets taken using the 5 kW PS, the 6 kW H6, and the 1.5 kW SPT-100 Hall effect thrusters in different test facilities to within the experimental uncertainty. When compared to predictions generated assuming ingestion by the random flux of neutral particles, the ingested flow rates computed by the background flow model are shown to be 40 to 70% closer to the empirical measurements without requiring any semiempirical inputs. It is also shown that the neutral ingestion at a fixed facility pressure can vary by as much as 91%, suggesting that background pressure magnitude is an insufficient parameter for fully describing neutral ingestion effects. These results indicate that the developed analytical background flow model is an effective predictive tool for computing neutral ingestion into Hall effect thrusters.

Nomenclature

A_{exit}	=	thruster exit plane area, m^2
F_{S+}	=	mass flow rate crossing surface S moving in the positive direction, kg/s
k	=	Boltzmann's constant, J/K
m	=	molecular mass of the background neutral, kg
\dot{m}	=	net mass flow rate of gas, kg/s
\dot{m}_b	=	net mass flow rate of bleed gas, mg/s
\dot{m}_{ing}	=	ingestion mass flow rate of the background neutrals, kg/s
n	=	number density, m^{-3}
n_b	=	background neutral number density, m^{-3}
n_p	=	number of active cryopumps
n_S	=	number density of particles crossing surface S , m^{-3}
n_{S+}	=	total number density of particles crossing surface S moving in the positive direction, m^{-3}
n_{S+i}	=	number density of particles of population i crossing surface S moving in the positive direction, m^{-3}
n_{S-i}	=	number density of particles of population i crossing surface S moving in the negative direction, m^{-3}
S	=	surface area, m^2
S_c	=	chamber cross-sectional area, m^2
S_{pd}	=	total surface area of downstream pump surfaces, m^2
S_{pe}	=	total surface area of end dome pump surfaces, m^2
S_{pu}	=	total surface area of upstream pump surfaces, m^2
s_d	=	ratio of total surface area of the downstream pump surfaces to the chamber cross-sectional area
s_e	=	ratio of total surface area of the end dome pump surfaces to the chamber cross-sectional area
s_u	=	ratio of total surface area of the upstream pump surfaces to the chamber cross-sectional area

T	=	gas temperature, K
T_b	=	temperature of the background neutrals, K
T_i	=	temperature of particles of population i , K
T_p	=	temperature of the pump surface, K
T_w	=	temperature of the chamber wall, K
V_i	=	thermal-diffusive velocity of particles of population i , m/s
V_s	=	thermal-diffusive velocity of particles crossing surface S , m/s
α	=	pump sticking coefficient
Φ	=	ingestion flux due to random motion of background neutrals, $\text{m}^{-2} \cdot \text{s}$

I. Introduction

THE high specific impulse, thrust efficiency, and thrust density provided by Hall effect thrusters (HETs) make them an appealing choice for use as the primary propulsion system on board increasing numbers of near-Earth satellite missions. In addition to the propellant mass savings offered by these performance attributes, developments in in-space power and the growing Western flight heritage portfolio of HETs have also increasingly made them prime candidates for more ambitious deep space missions [1–3].

The interest in these devices has caused a corresponding increase in the quantity of HET research and testing at numerous vacuum facilities. Despite the physical similarities among the HETs operated and characterized at each of these facilities, the wide range of facility geometries, sizes, materials, and pumping capacities makes it difficult for researchers to compare datasets without the inclusion of facility-dependent corrections [4]. It is therefore necessary to develop an understanding of how to quantify ground-based vacuum facility effects on measured HET operation, thrust performance, and plume characterization so that facility-dependent testing artifacts can be corrected for and a facility-independent understanding of HET performance can be achieved.

Existing investigations focused on HET facility effects primarily focus on the impact of facility backpressure on plume properties and device performance. Previous studies have shown that increases in facility pressure result in artificial increases in device thrust and efficiency [5–21]. This observed performance augmentation has been attributed to the ingestion of background neutrals present in the vacuum facility [5–21]. In this process, background neutrals are entrained by the HET and used as propellant; thus, these neutrals are subsequently ionized and accelerated upon being ingested, but they are not accounted for as part of the anode flow rate directly supplied to the HET [5–21]. In many of these previous investigations, the entrainment of background neutrals is treated as the result of the random flux of these neutrals across the exit plane of the thruster

Received 23 March 2016; revision received 16 October 2016; accepted for publication 31 October 2016; published online 30 January 2017. Copyright © 2016 by Jason David Frieman. Published by the American Institute of Aeronautics and Astronautics, Inc., with permission. All requests for copying and permission to reprint should be submitted to CCC at www.copyright.com; employ the ISSN 0748-4658 (print) or 1533-3876 (online) to initiate your request. See also AIAA Rights and Permissions www.aiaa.org/randp.

*Graduate Research Assistant, Aerospace Engineering, High-Power Electric Propulsion Laboratory; jfrieman3@gatech.edu. Student Member AIAA.

†Research Engineer II, Aerospace Engineering, High-Power Electric Propulsion Laboratory; thomas.liu@ae.gatech.edu. Member AIAA.

‡Associate Professor, Aerospace Engineering, High-Power Electric Propulsion Laboratory; mitchell.walker@ae.gatech.edu. Associate Fellow AIAA.

(hereafter referred to as the thermal model) [8,9,13,15,17,21]. In the thermal model, the corresponding ingestion flux of background particles Φ can be expressed as a function of Boltzmann's constant k as well as the number density n_b , temperature T_b , and molecular mass m of the background neutrals using the following equation [8,9,13–15,21]:

$$\Phi = \frac{1}{4} n_b \sqrt{8kT_b/\pi m} \quad (1)$$

The corresponding ingested mass flow rate of neutrals into the HET \dot{m}_{ing} can then be found as the multiplicative product of the ingestion flux from Eq. (1), the molecular mass of the background gas, and the thruster exit plane area A_{exit} , as shown in Eq. (2) [13,21]:

$$\dot{m}_{\text{ing}} = \Phi m A_{\text{exit}} \quad (2)$$

The thermal model has been successfully applied to explain trends observed in early empirical measurements of the SPT-100 HET and was used to generate the recommendation that all HETs be tested at a facility pressure below 5.0×10^{-5} Torr in order to keep background neutral ingestion below the threshold required to generate reliable predictions of in-orbit performance [13,17]. However, subsequent investigations with different HETs in different facilities have shown that the results generated by the thermal model underpredict the empirically observed changes in discharge current (for cases of constant anode mass flow rate), required anode flow rate (for cases in which the discharge current was held constant), or thrust [8,9,14–16,21]. Specifically, previous studies have shown that the ingestion mass flow rates predicted by the thermal model are 2–14 times too small to account for empirical observations [14,16,21]. These underpredictions have prompted proposals replacing the exit plane area in Eq. (2) with a larger effective ingestion area to account for ionization of background neutrals in regions of the near-field plume where the electron temperature is still high enough to ionize neutral gas [11,14,15]. This approach has been disputed due to its reliance on the assumption that neutrals ingested across a reference surface in the plume are ionized equivalently to neutrals supplied through the HET gas distributor [6,15]. Furthermore, although successfully applied to data taken with the 6 kW H6 in the large vacuum test facility (LVTF) at the University of Michigan, this approach has not yet been shown to be broadly applicable across multiple devices and facilities [6,15]. Overall, these shortcomings prevent an accurate determination of HET flow ingestion, and thus hinder the ability to accurately gauge changes in HET operating characteristics as a function of ingestion flow rate [8,9,14–16,21].

In addition to the aforementioned shortcomings, the thermal model assumes that all motion of background neutrals is random in nature. However, previous work modeling the rarefied background flow

inside a HET test facility found that the background neutrals could not be treated simply as a static gas field with only thermal velocity components [22–24]. Instead, it was found that an organized background flowfield existed within the test facility during HET operation and that bulk axial velocities of over 100 m/s were achieved by the background neutrals [22,23]. These models were successfully used to replicate the empirically observed spatial pressure distribution within the LVTF as well as the VF-5 vacuum facility at NASA John H. Glenn Research Center; however, only limited attempts have been made to apply these concepts to assess how the bulk flow of background neutrals could impact HET ingestion as well as explain previously acquired HET facility effects data.

This paper uses the bulk background flow modeling concepts first proposed by Cai et al. in order to predict the ingestion of background neutrals by a HET [22]. The original model of the LVTF created by these researchers is further developed in order to accommodate facilities with different physical geometries and pump placements as well as directly compute the expected ingested mass flow rate of background neutrals by a given HET. The predictions of this expanded model are then compared to previous empirical datasets collected with three different thrusters in two different vacuum test facilities in order to evaluate the ability of the model to successfully predict empirical data. Finally, the background flow model is used to assess the impact of facility pump configuration and the pressure modulation technique on neutral ingestion mass flow rate. This includes a sensitivity analysis focused on determining how the model predictions are affected by the assumptions used to develop it (e.g., the temperatures of the chamber wall and pump surfaces, the pump sticking coefficient, etc.). It is important to note that, for completeness, the preceding introduction cites previously referenced results from existing publications (both archival and nonarchival) on HET facility effects and neutral ingestion.

II. Background Flow Model

A. Overview of HET Vacuum Test Facilities

Figure 1a shows a schematic of a typical vacuum test facility used for HET testing. These test facilities are usually stainless-steel cylindrical vacuum chambers measuring 4 m or more in length and 2 m or more in diameter, equipped with cryopumps in order to achieve and maintain operating pressures on the order of 10^{-5} Torr or less [6,22,25–27]. The cryopumps operate by cooling a plate or series of plates to an operating temperature of approximately 15 K using gaseous helium [22]. When incident particles strike the pump surface, a fraction of the particles is condensed onto to the pump surface while the remaining particles reflect with a thermal speed characterized by the pump surface temperature [22]. The probability that incident particles are condensed on the pump surface is known as the sticking coefficient α , with the probability that an incident particle

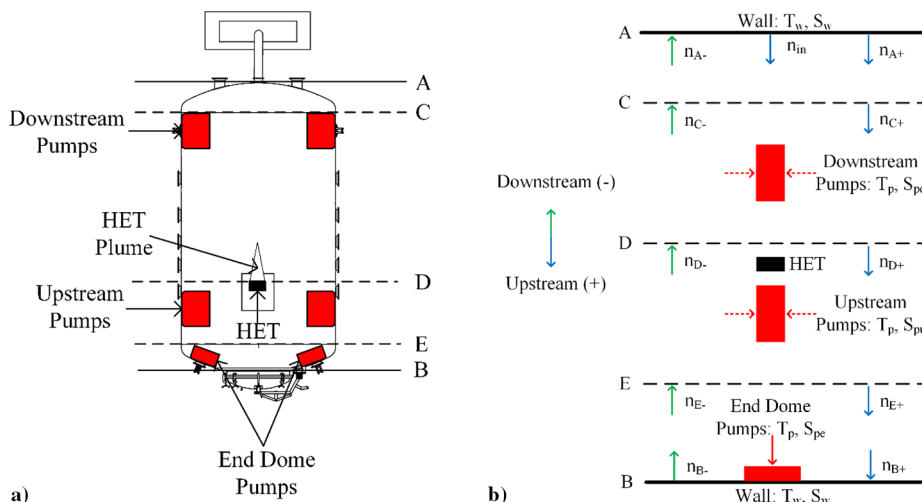


Fig. 1 A typical HET test facility a) schematic and b) background flow model representation.

reflects off the pump expressed as $1 - \alpha$ [22]. Thus, the sticking coefficient is a metric of pump performance and quantifies how effectively the pumps act as sinks of neutral particles from the background flowfield [22]. The number and location of these pumps vary between different facilities, as does the facility geometry [6,22,28].

In operation, a HET is mounted inside the vacuum facility to a test stand typically located at one end of the facility. A low-density plasma flow (i.e., the HET plume) is then exhausted from the thruster in the axial direction toward the downstream end of the facility. Although some of the emitted ions and electrons recombine before striking the downstream facility surfaces, the ion–electron recombination mean free path is generally longer than the characteristic axial facility dimensions; thus, most of these charged particles strike the downstream facility surfaces, recombine, and reflect as neutrals with a thermal speed characterized by the chamber wall temperature [22,25,28]. Upon reflection, these neutrals are then able to traverse the vacuum facility until they strike and are condensed on one of the cryopumps. This motion of neutrals through the vacuum facility is known as the background neutral flow and is the focus of this model.

B. Assumptions and Basic Relations

1. Assumptions

To model the flow environment described previously, several simplifying assumptions were made. These assumptions, as well as the corresponding justifications underlying them, are detailed below.

The first set of assumptions concerns the background flow environment. First, it is assumed that the background flow in the test facility is in the free molecular regime. Previous work has shown that, because HET test facilities typically operate at pressures of 10^{-5} Torr of xenon (Xe) or below, the Knudsen number in these facilities is of order unity [22]. This is well within the range considered to be characteristic of a free molecular flow environment [29]. It is also assumed that the background flow is one-dimensional along the thrust axis of the HET. This assumption is consistent with previous studies into background neutral flows, which have yielded good agreement with more complex numerical simulations and empirical measurements [22,30]. The accuracy of the one-dimensional (1-D) assumption is further examined in Sec. IV.E. Finally, it is assumed that the background flow is in thermodynamic equilibrium. This implies all variables that impact the background flow (i.e., the temperatures of the chamber wall and pump surfaces as well as the anode mass flow rate) are in steady state. This restricts the model to predictions of time-averaged ingestion flow rates. This restriction is appropriate for this model because the focus is on replicating empirical results acquired on the timescale of seconds to minutes (i.e., measurements of average discharge current and thrust) and not on the oscillation characteristics of HETs that occur at characteristic frequencies on the order of 20 kHz [31].

The next set of assumptions pertains to the vacuum test facility. Within the model, the chamber wall temperature and pump surface temperature are assumed to be constant and equal to 300 and 15 K, respectively. For this work, the term “pump surface temperature” refers to the temperature of the helium cryosail and not the temperature of any liquid-nitrogen-cooled shrouds. The assumed pump surface temperature is consistent with reported empirical measurements in HET test facilities [26]. Furthermore, all cryopumps are assumed to have a constant sticking coefficient of 0.4. It is important to note that typical values for the sticking coefficient of noble gases on bare cryogenic panels are typically within a range of 0.6–0.8 [32]. However, because the pumps installed in many HET test facilities are surrounded by liquid-nitrogen-cooled louvered shrouds, the effective sticking coefficient for these pumps can be lower than the values achieved for a bare cryosurface; the assumed sticking coefficient of 0.4 is in agreement with previous analytical and empirical studies of cryosurfaces with louvered shrouds [22,26]. The sensitivity of the model to these assumptions is assessed in Sec. IV.D.

The final set of assumptions concerns the behavior of the individual particles composing the HET plume and background flow.

First, it is assumed that neutrals fully accommodate to the surfaces they strike and reflect specularly. Previous analysis has shown that the differences in results generated between diffuse and specular reflection assumptions are small; thus, the impact of this assumption is expected to be minor [30]. Next, it is assumed that all particles injected into the HET anode travel unimpeded to the downstream facility surfaces, thermalize, and reflect. Thus, the downstream facility surfaces are considered as a source of neutral xenon entering the chamber at the thruster anode mass flow rate, through the chamber cross-sectional surface area, and at the wall temperature. This assumption is consistent with previous work into background flow modeling in HET test facilities [22]. It is furthermore supported by empirical measurements of the velocity distributions within HET plumes; these measurements show that both ions and neutrals exhausted by the HET have large axial velocity components in the direction of the downstream chamber surfaces [33]. Further empirical evidence indicates that the majority of the ions are unlikely to undergo a recombination collision before reaching the downstream facility surfaces [28]. Thus, the most likely pathway for these particles to begin traveling back toward the thruster is by reflection from the downstream facility surfaces. It is nevertheless important to note that this assumption does not capture two processes present in facilities with downstream pumping surfaces. First, it does not capture the loss of unionized propellant exhausted by the HET due to contact with pump surfaces during the initial transit from the HET to the downstream facility surfaces. Second, it does not capture the effective reduction in chamber area caused by the shadowing of these downstream surfaces by the cryopumps. Fortunately, these processes have offsetting effects on the number density. Specifically, the first process reduces the effective inflow number density, whereas the second increases it.

Finally, it is assumed that the HET plume flow collisionally scatters background flow neutrals traveling toward the HET exit plane. The only collisions that are considered are the elastic collisions between the background neutrals and the unionized propellant exhausted by the HET. The collisional cross sections are computed using models employed in previous HET plume models [34]. To compute the cross sections, it is assumed that the neutral density at the exit planes of all HETs is approximately $1 \times 10^{18} \text{ m}^{-3}$; this estimate is taken from previous empirical measurements using the 1.5 kW SPT-100 and 5 kW P5 HETs, both of which are used as points of comparison for this work [34,35]. The neutral density is furthermore assumed to follow an inverse-square dependency; this variation is derived by modeling the neutral density as the isotropic emissions of a rarefied flow from a disk with a diameter equal to the thruster exit area, and is commonly applied in HET plume models [7]. The velocity of plume neutrals is taken to be approximately 200 m/s, which is consistent with previous empirical measurements [33]. It is important to note that the large relative velocity (i.e., greater than 20,000 m/s) between the ions exhausted by the HET and the background neutral flows results in an elastic collisional cross section more than an order of magnitude smaller than the computed cross section for the elastic collisions between the background neutrals and the unionized propellant exhausted by the HET; thus, this ion-neutral collision process is ignored for this work.

2. Basic Relations

Before the background flow model can be mathematically developed, a few basic relations regarding the flow of rarefied gas in equilibrium must be presented. The net mass flow rate \dot{m} of a rarefied gas across a surface in one direction for a one-dimensional flow is given by Eq. (3):

$$\dot{m} = mn_s S \sqrt{(8kT)/(\pi m)} / 4 = mn_{s+} S \sqrt{(2kT)/(\pi m)} \quad (3)$$

where S is the area of the surface, T is the temperature of the particles crossing the surface, n_{s+} is the number density of particles crossing surface S moving in the positive direction (which is equal to half the total number density of particles at the surface because there are only two potential directions of motion), and all other variables retain their

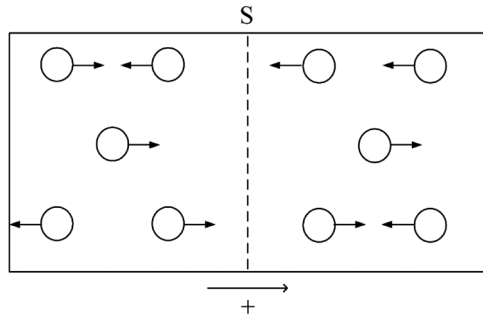


Fig. 2 One-dimensional motion of a rarefied gas.

meaning from previous equations [22]. The situation described by Eq. (3) is illustrated in Fig. 2.

For convenience, the simplified thermal-diffusive velocity term V_s from Eq. (3) will be defined as shown in Eq. (4):

$$V_s = \sqrt{(2kT)/(\pi m)} \tag{4}$$

Finally, from the law of mass conservation and Eq. (3), the number of particles of incoming temperature T_1 reflected from a surface at a different temperature T_2 is given by Eq. (5) [22]:

$$n_1 \sqrt{T_1} = n_2 \sqrt{T_2} \tag{5}$$

In Eq. (5), n_1 is the number density of the incoming particles and n_2 is the number density of the reflected particles.

C. Model Development

Using the assumptions from Sec. II.B.1, the typical HET test facility shown in Fig. 1a is transformed into the 1-D background flow model shown in Fig. 1b. To help correlate the model to the test facility, identical reference surfaces are drawn on both the schematic of the HET chamber shown in Fig. 1a and the model representation in Fig. 1b. These reference surfaces demarcate the different chamber regions of interest: the downstream wall region is located between surfaces A and C, the downstream pump region is located between surfaces C and D, the upstream pump region is located between surfaces D and E, and the end dome pump region is located between surfaces E and B. For this work, the dividing line between the upstream and downstream regions is the HET exit plane. In other words, all pumps located downstream of the HET exit plane and not on the end domes of the vacuum test facility are considered to be in the downstream pump region, whereas those located upstream of the HET exit plane and not on the end domes of the vacuum test facility are considered to be in the upstream pump region. As shown in Fig. 1b, because the model is one-dimensional, the number density of particles (and the corresponding flux) crossing each of these surfaces can be further decomposed into an upstream (i.e., positive) and a downstream (i.e., negative) component.

The analytical model needed to compute the ingestion flow rate due to the background neutral flow is built from the identified assumptions, basic relations, and modeling domain. To arrive at this final solution, expressions for the flux and number density of background neutrals crossing each of the surfaces in both directions need to be obtained. These expressions can then be combined into a system of equations that can be solved for the ingestion number density n_{D+} and mass flow rate F_{D+} . The model will be presented region by region in order to explicitly show the unique aspects associated with each type of region. Furthermore, the resulting equations will compose a toolkit that can readily be applied to build a model of any facility geometry or pump configuration.

1. Pump Regions

The model development starts by examining the flow environment in the upstream and downstream pump regions. There are three potential outcomes for background particles that enter a pump region:

- 1) The particles can proceed unimpeded through the region and exit at the temperature with which they entered.
- 2) The particles can strike a pump and condense, which removes them from the flow.
- 3) The particles can strike a pump and reflect at the pump temperature.

These outcomes are shown in Fig. 3.

Thus, the flow rate of particles of population i exiting the pump region F_{D+i} can be written as follows [22]:

$$F_{D+i} = mS_c n_{C+i} V_i - mS_{p_d} n_{C+i} V_i + (1 - \alpha) n_{C+i} S_{p_d} m V_p \sqrt{T_i/T_p} \tag{6}$$

Note that Eq. (6) is written using the flux across surface D in the positive direction as an example exit surface from a pump region. In Eq. (6), S_c is the chamber cross-sectional area, S_{p_d} is the total surface area of cryopumps located in the relevant pump region (for this example, it would be the downstream pump region), n_{C+i} is the number density of particles of population i entering the pump region (that, for this example, would be the number density of particles of population i crossing surface C in the positive direction), V_i is the thermal-diffusive speed characterized by the temperature of particles of population i (T_i), V_p is the thermal-diffusive speed characterized by the pump surface temperature T_p , and all other terms retain their meanings from previous expressions.

Each of the summation terms in Eq. (6) represents one of the possible outcomes discussed previously. The first term represents particles that traversed the pump region unimpeded; the second term represents the particles that struck a pump surface and condensed; and the third term represents the fraction of particles that struck a pump surface but did not condense, and instead reflected at a thermal-diffusive speed characterized by the pump surface temperature. Finally, it is important to note that Eq. (6) is also written for a single population of particles. If additional populations are entering the pump region, then Eq. (6) will be applied to each population and the total exit flow rate will be equal to the sum of the exit flow rates for each population. Such a situation could arise for adjacent pump regions (i.e., the upstream and downstream pump regions for a chamber similar to the one shown in Fig. 1a) because, after traversing the first pump region, the flux entering the second pump region would be composed of a population of particles at the original entry temperature and another at pump surface temperature made up of those particles that struck but were not trapped by a pump in the first pump region.

The number density of particles of population i exiting the pump region n_{D+i} can similarly be written as follows [22]:

$$n_{D+i} = (1 - s_d) n_{C+i} + (1 - \alpha) n_{C+i} s_d \sqrt{T_i/T_p} \tag{7}$$

In Eq. (7), s_d is the ratio of pump surface area to facility cross-sectional area in the region of interest, and all other terms retain their meaning from previous expressions. The first term of Eq. (7)

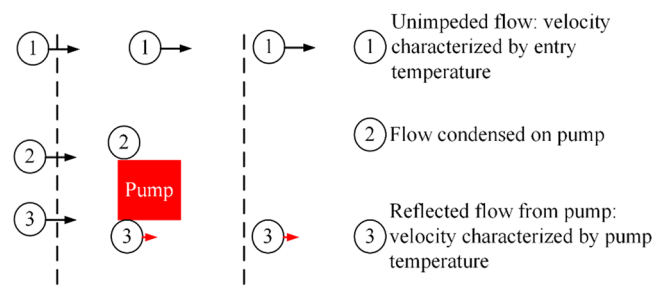


Fig. 3 Three potential outcomes for particles in pump regions.

represents the number density of particles that proceeded unimpeded through the pump region, whereas the second is the number density of those that reflected from a pump and are now moving at a thermal-diffusive speed characterized by the pump surface temperature. As with Eq. (6), Eq. (7) is written for a single population of particles, and the total exit number density would be equal to the sum of the number densities for each population.

2. Wall Regions

The next class of regions to consider includes wall regions without end dome pumps. Such a region is shown between surfaces C and A in Fig. 1b. All particles entering this region strike the facility walls, thermally accommodate to the facility wall, and then reflect with a thermal-diffusive speed characterized by the facility wall temperature. This process is shown in Fig. 4.

The resulting exit flow rate can be expressed as follows [22]:

$$F_{C+i} = mS_c n_{A-i} V_w \sqrt{T_i/T_w} \tag{8}$$

The corresponding exit number density is as follows [22]:

$$n_{C+i} = n_{C-i} \sqrt{T_i/T_w} \tag{9}$$

In Eqs. (8) and (9), V_w is the thermal-diffusive speed characterized by the temperature of the chamber wall T_w and all other variables retain their meaning from previous expressions. As with Eqs. (6) and (7), both Eqs. (8) and (9) must be applied to all populations present, and the total mass flow rates and number densities will be the sum of the contributions of all populations and any source terms.

3. End Dome Pump Regions

The final type of facility region is an end dome pump region. Such a region is shown between surfaces E and B in Fig. 1b. Particles entering this region can either 1) strike and thermally accommodate to the facility wall then reflect with a thermal-diffusive speed characterized by the facility wall temperature; 2) strike an end dome pump and condense; or 3) strike and thermally accommodate to an end dome pump, and then reflect with a thermal-diffusive velocity characterized by the pump surface temperature. These outcomes are illustrated in Fig. 5.

Thus, the number density of particles of population i exiting the end dome pump region n_{E-i} can be written as follows:

$$n_{E-i} = (1 - s_e)n_{E+i} \sqrt{T_i/T_w} + (1 - \alpha)n_{E+i} s_e \sqrt{T_i/T_p} \tag{10}$$

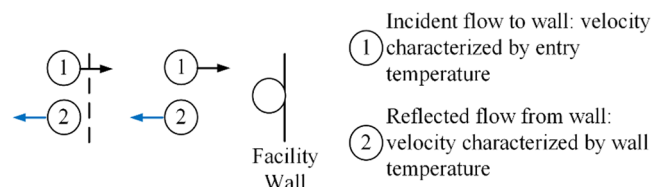


Fig. 4 Illustration of outcome for particles in wall regions.

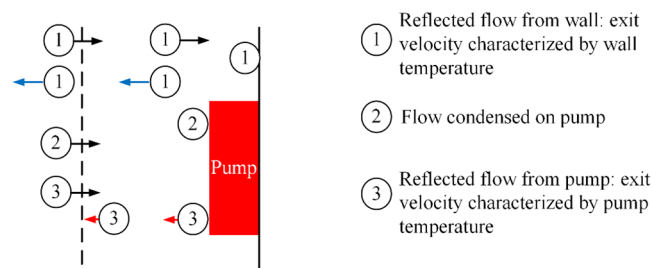


Fig. 5 Three potential outcomes for particles in end dome pump regions.

In Eq. (10), s_e is the ratio of pump surface area to facility cross-sectional area in the end dome pump region, and all other terms retain their meaning from previous expressions. The first term of Eq. (10) represents the number density of particles that strike the facility wall and are reflected with a thermal-diffusive speed characterized by the facility wall temperature, whereas the second term is the number density of reflected particles from a pump that are now moving at a thermal-diffusive speed characterized by the pump surface temperature.

4. Final Expressions

Application of Eqs. (7), (9), and (10) to each of the reference surfaces shown in Fig. 1b results in a system of equations that can be solved simultaneously for the directional number densities crossing each surface. This system is shown for the positive directional number densities in Eqs. (11–13). A similar system can be developed for the negative number densities crossing each surface:

$$n_{D+} = (1 - s_d)n_{C+} + (1 - \alpha)s_d n_{C+} \sqrt{T_w/T_p} \tag{11}$$

$$n_{E+} = n_{B+} = (1 - s_u)(1 - s_d)n_{C+} + (s_u(1 - s_d) + (1 - s_u)s_d + s_u(1 - \alpha)s_d)(1 - \alpha)n_{C+} \sqrt{T_w/T_p} \tag{12}$$

$$n_{C+} = n_{A+} = n_{in} - n_{C+}(\alpha s_d - 1)^2(\alpha s_e - 1)(\alpha s_u - 1)^2 \tag{13}$$

Because the HET exit plane is located just upstream of surface D, the parameter of interest for HET neutral ingestion is the mass flow rate of particles crossing surface D in the upstream direction F_{D+} . The solution for this parameter is shown in Eqs. (14) and (15):

$$n_{C+} = \frac{n_{in}}{1 + (\alpha s_d - 1)^2(\alpha s_e - 1)(\alpha s_u - 1)^2} \tag{14}$$

$$F_{D+} = mS_c n_{C+} V_w - mS_{p_d} n_{C+} V_w + (1 - \alpha)n_{C+} S_{p_d} mV_p \sqrt{T_w/T_p} \tag{15}$$

$$n_{in} = \frac{\dot{m}_{a,p}}{S_c} \tag{16}$$

In Eqs. (11–15), s_u is the ratio of pump surface area-to-facility cross-sectional area in the upstream pump region, and all other terms retain their meaning from previous expressions. In Eq. (14), n_{in} is the input number density due to the HET anode flow computed as per the assumption regarding plume flow reflection in Sec. II.B.1. For clarity, this parameter is shown expressed as a function of the anode particle flow rate $\dot{m}_{a,p}$ and the chamber cross-sectional area in Eq. (16). Because the HET exit plane occupies only a small fraction of the cross-sectional area of surface D, computing the actual ingested mass flow rate due to the background neutral flow requires the mass flow rate computed in Eq. (15) to be scaled by the ratio of the HET exit plane area to the cross-sectional area of the facility. This scaling ensures that only those particles that are on a trajectory to enter the HET channel are counted as part of the ingested mass flow rate.

Although developed for the chamber shown in Fig. 1a, Eq. (14) can readily be modified to accommodate chambers of different geometric sizes and pump configurations by appropriately modifying the values of s_e , s_u , and s_d . For example, the result for a facility with no end dome pumps would be equal to Eq. (14) evaluated with s_e set to zero. Similarly, thrusters of different sizes or operating conditions can be accommodated by appropriately adjusting the exit area in the scaling mentioned previously and the source term in Eq. (14).

As an initial test case, the aforementioned approach was applied in order to generate the form of Eq. (14) relevant to a facility with upstream pumps only. Such a facility matches the original model developed for the LVTF by Cai et al. [22]. By setting both s_e and s_d to

zero (i.e., by removing the downstream and end dome pumps from the model), the empirically validated expression developed by Cai et al. is indeed recovered [22]. As an additional test case, the background flow model was used to compute the number density of particles crossing surface D in the positive direction, assuming that both s_d and α were equal to one. This situation represents the limiting case of finding the number density remaining after a rarefied flow passes into a region occupied entirely by a pump surface onto which all incident particles condense. As expected, the model predicts that no particles would exit this region. These two test cases confirm both the accuracy of the math underlying the model and the aforementioned approach in expanding the background flow model to accommodate a wider variety of facility configurations.

Now that the final expressions of the model are developed, it is important to revisit the physical processes captured by Eqs. (14) and (15) and how these processes might explain the empirically observed enhancement in background neutral ingestion relative to the predictions of the thermal model. As described in detail in Sec. II.A, the physical process captured by this model is the reflection of the low-density plasma flow (as neutrals) from the downstream facility surfaces and their subsequent axial motion back toward the HET. This reflected motion is caused by the finite axial dimensions and pumping speed of the facility and represents a bulk motion toward the HET exit plane that could result in an additional or enhanced ingestion flux into the HET beyond that captured by the random motions of the thermal model. It is this additional flux (of the flow reflected off the downstream facility surfaces) that is captured by Eq. (15) and the concomitant enhancement of local number density that is captured by Eq. (14). Specifically, the velocity terms in Eq. (15) represent the bulk axial velocity of neutrals toward the HET exit plane due to reflection off of the facility surfaces.

It is furthermore important to note that this reflective process is not unique to HETs, but it is widely applicable to any directional flow of a low-density plasma in a finite vessel including the plume produced by gridded ion engines during ground testing. However, unlike in HETs (which have open channel exit areas in which ions are created), neutral ingestion into gridded ion engines is conductance limited by the grid apertures [7]. Thus, the bulk background flow is not able to freely stream into the ion engine discharge chamber and contribute to the plasma generation in this region. This significantly limits the impact of the bulk background flow on the ingestion characteristics of gridded ion engines and suggests the thermal model is sufficient for correcting the data acquired from these devices, despite the model approximations [7].

5. Comparisons to Existing Background Flow Models

Although the model developed in the preceding sections follows a similar approach to that taken by Cai et al., it differs from this original model in several important ways [22,30,36]. First, all models developed by Cai et al. have only a single pump region with a single type of pump (i.e., either end dome pumps exposed to the flow on only one side or upstream/downstream pumps exposed to the flow on two sides) [22,30,36]. Because of this, in those models, all particles enter the pump region with a uniform velocity characterized by the temperature of the facility walls [22,30,36]. In contrast, the model developed in this work allows for the possibility of several adjoining pump regions of different types, and thus the entrance of particles of several different populations with several different velocities into these regions. The ability to model adjoining pump regions and the corresponding discussion of how to account for these different populations is thus unique to this model and represents an increase in complexity over the original models developed by Cai et al. [22,30,36]. In addition, none of the original 1-D flow models created by Cai et al. accounted for the collisional scattering processes associated with the interaction of the background flow with the HET plume [22,30,36]. These processes are accounted for in this work as described in Sec. II.B.1. It is important to note that many of the additional complexities accounted for in this model are also accounted for in the more complex direct simulation Monte Carlo (DSMC) models of the background flow environment in ground test facilities developed by Yim and Burt [23] and Nakayama and

Nakamura [24]. However, in contrast to these DSMC models, the proposed 1-D model is much simpler to implement and customize to fit a given thruster and facility combination. To compare the two approaches (and therefore preliminarily assess the viability of the employed simpler approach), the background flow model is used to compute the weighted average speed of neutrals crossing surface D (i.e., those neutrals nearest the HET). These computations show a most probable speed of approximately 100 m/s, which is in good agreement with the velocity distribution functions generated by the more complex DSMC codes [23].

The final difference between the model developed in this work and those previously developed lies in the application of the model results. The models developed by Cai et al. [22,30,36], Yim and Burt [23], and Nakayama and Nakamura [24] were all used to create maps of the spatial neutral pressure distribution within ground test facilities. Although these results also indicated the presence of a bulk background flow of neutrals toward the thruster, to date, none of these models have been applied to compute the resultant ingestion mass flow rate into the HET due to this bulk motion, nor have they been used to replicate existing empirical datasets quantifying the sensitivity of HETs to background pressure.

III. Comparisons to Empirical Data

To validate the applicability of the background flow modeling approach for predicting neutral particle ingestion by HETs, the model developed previously was used to compute the ingested mass flow rates for situations identical to several published experimental works on HET facility effects. These results were then compared against the empirical measurements of ingestion flow rate as well as the predictions of the thermal model.

When comparing the results of the background flow model to empirical measurements, it is assumed that background neutrals particles ingested by the HET are ionized equivalently to neutrals supplied by the gas distributor. This simple ingestion approach is similar to that taken in many previous works on facility effects and is consistent with the approach taken in all of the works used for comparison [8,9,14–16,21]. Furthermore, as mentioned previously, only neutral particles that cross the HET exit plane and enter the discharge channel are counted as part of the ingested mass flow rate in the background flow model. Because the mass flow in this region of the channel is free molecular, these neutral particles are free to travel into the ionization zone of the HET, and are thus subject to collisions with the high-temperature electrons within this zone, as are the neutrals supplied by the gas distributor [14].

A. P5 HET in the LVTF

The first data used for model validation were collected using the P5 HET in the LVTF at the University of Michigan. The P5 is a laboratory-model Hall thruster developed jointly by the U.S. Air Force Research Laboratory (AFRL) and the University of Michigan [21]. The P5 has a nominal operating power of 5 kW [21]. The LVTF is a stainless-steel clad vacuum chamber measuring 9 m in length and 6 m in diameter, and it is equipped with seven cryopumps located upstream of the HET test station for a combined total upstream pump surface area of 7.26 m² [8,21,22].

The first dataset used for validation was acquired by Hofer et al. [8]. In this work, the anode mass flow rate supplied to the P5 was varied in order to maintain a constant discharge current as the number of active pumps in the LVTF was varied from four to seven [8]. The authors noted that higher anode mass flow rates were required to achieve a given discharge current at lower facility pressures and attributed the resultant change in the required anode mass flow rate to a decrease in neutral ingestion [8]. For instance, approximately 10 mg/s of anode flow was required, on average, to achieve a discharge current of 10 A in the four-pump configuration; whereas 10.21 mg/s of anode flow was required, on average, in order to achieve the same discharge current in the seven pump configuration [8]. Thus, the change in the ingested mass flow rate between the two conditions could be approximated as 0.21 mg/s. The background flow model was similarly used to compute the difference in ingestion flow rate for the P5 in the LVTF as

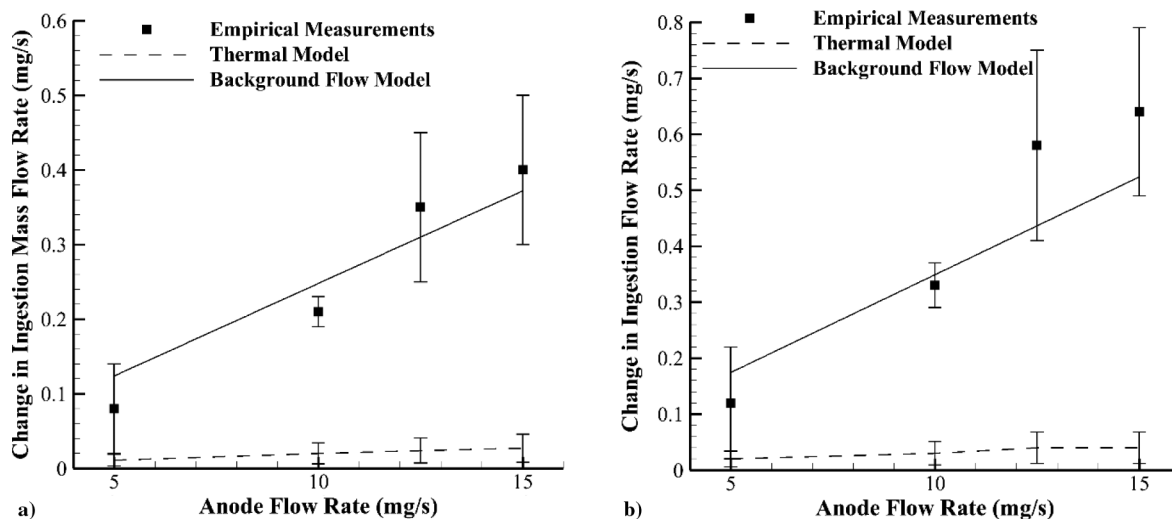


Fig. 6 Change in P5 ingestion flow rate between a) four and seven cryopumps, and b) seven cryopumps and vacuum.

the number of active cryopumps was changed from four to seven. The results are shown as a function of anode flow rate along with the empirical results in Fig. 6a. Also shown in Fig. 6a are the changes in ingestion flow rate predicted by the thermal model. Consistent with the approach taken by Hofer et al., the number densities used for the thermal model calculations corresponded to the average of the values acquired by a pair of hot-cathode ion gauges: one was located on the wall of the LVTF near the exit plane of the HET, and the other was located on the wall at an axial distance equal to half the length of the LVTF [8]. Previous work has shown that the pressures reported at these two locations in the LVTF varied by an average of 70%; the error bars shown for the thermal model predictions correspond to the uncertainty in the thermal model computations associated with this variance in the pressure measurements [37]. The error bars shown for the empirical data in the figure correspond to the reported uncertainty of the measurements.

As shown in Fig. 6a, the changes in the ingestion flow rate predicted by the thermal model are 7–15 times smaller than the empirical observations. However, the computed changes in the ingestion flow rate generated by the background flow model are within the empirical error bars for all but one of the anode flow rates. For that flow rate (10 mg/s), there is less than a 10% difference between the upper uncertainty bound and the prediction of the background flow model. Thus, for this dataset, the predictions generated by the background flow model are, on average, 70% closer to the empirical values than the predictions generated by the thermal model.

It is important to note that the background flow model consistently overpredicts the change in ingestion mass flow rate for the 5 and 10 mg/s anode flow rates, but it underpredicts this change for the 12.5 and 15 mg/s anode flow rates. The reason for this is likely due to the employed collision model. As noted in Sec. II.B.1, neutral particles exhausted by the HET are assumed to travel at a constant speed, regardless of the HET operating condition. However, the HET wall and anode temperatures have been empirically shown to increase with increasing discharge power [38]. This results in a corresponding increase in the temperature (and thus velocity) of unionized neutrals exhausted by the HET, with corresponding reduction in the collisional cross-section for the modeled elastic collisions between the background neutrals and the unionized propellant exhausted by the HET [39,40]. Because the background flow model does not capture this change in cross section, it overpredicts the number of collisions that a background neutral undergoes (and thus underpredicts the ingestion flow rate) for operating conditions with high anode flow rates, and vice versa for the low anode flow rate conditions.

To estimate the difference in operating characteristics between the LVTF and test conditions with no background pressure, Hofer et al. used the aforementioned data to generate linear fits that could be extrapolated to predict the anode flow rate that would be required to

achieve a given discharge current in true vacuum conditions [8]. The difference between this value and the anode flow rate required to achieve the same discharge current in the LVTF represents the ingested flow rate of neutrals by the P5 in the LVTF with all seven cryopumps operating. The background flow model was similarly used to compute the ingestion flow rate for the P5 in the LVTF with all seven pumps on. The results are shown as a function of the anode flow rate along with the empirical results in Fig. 6b. As done by Hofer et al., the empirical data shown in Fig. 6b represent the average of the values acquired for each flow rate across four discharge voltages, whereas the error bars correspond to the standard deviation of these values [8]. Also shown in the figure is the ingestion flow rate predicted by the thermal model for the P5 in the LVTF with all seven cryopumps operating. The number densities used for the thermal model calculations were determined identically to the procedure described for the data shown in Fig. 6a [8].

As was the case for the data shown in Fig. 6a, the results shown in Fig. 6b indicate that the predictions made by the background flow model are significantly closer to the empirical observations than the predictions generated using the thermal model. Specifically, the ingestion flow rates predicted by the thermal model are 11–24 times smaller than the empirical observations. By contrast, the difference between the estimates generated by the background flow model and the empirical measurements is less than the empirical error for all of the tested anode flow rates.

The next empirical dataset used to validate the background flow model was acquired by Walker and Gallimore using the same thruster and test facility [21,26]. In this work, the anode mass flow rate supplied to the P5 was held constant and the resultant discharge current was measured as the number of active pumps in the LVTF was varied from two to four to seven [21,26]. The authors noted that higher discharge currents were observed at higher facility pressures and attributed the resultant change in discharge current to an increase in neutral ingestion [21,26]. For instance, the discharge current of the P5 operating at a discharge voltage of 400 V and an anode flow rate of 5.25 mg/s was observed to be approximately 5 A with seven cryopumps on and 5.2 A with four cryopumps on. Using flow unit conversions, it can be shown that single ionization of 1 mg/s of xenon flow results in approximately 0.7 A of ion current [7]. In HETs, the ratio of the ion beam current to the discharge current is typically on the order of 70% and has been shown to remain close to this value even at elevated ingestion flow rates; thus, an increase in ion current of approximately 0.7 A should result in a concomitant increase of 1 A in the discharge current [19,41]. Thus, the observed change of 0.2 A of discharge current can be approximated as being due to a 0.2 mg/s reduction in ingestion mass flow rate between the four and seven cryopump configurations. It is important to note that this conversion is a rough approximation as compared to the direct measurements of anode flow changes acquired by Hofer et al. [8].

To quantify the error associated with this approximation, the average percent difference between the P5 discharge current predicted using the aforementioned flow rate to discharge current conversion and those measured empirically was computed for all of the discharge voltages and flow rates used by Walker and Gallimore [21]. The average percent difference between the estimated and empirical results is approximately 1%, which approximates the overall error associated with the employed estimation technique.

The background flow model was similarly used to compute the difference in ingestion flow rate for the P5 in the LVTF as the number of active cryopumps was changed from two to seven. The results are shown as a function of anode flow rate along with the empirical results in Fig. 7. Consistent with the approach of Hofer et al. [8], the empirical data shown in Fig. 7 represent the average of the values acquired for each flow rate across four discharge voltages, whereas the error bars correspond to the standard deviation of these values. Also shown in the figure are the changes in ingestion flow rate predicted by the thermal model. Consistent with the approach taken by Walker and Gallimore, the number densities used for the thermal model calculations correspond to the empirical measurements taken using a single hot-cathode ionization gauge located on the wall of the LVTF downstream of the HET test station [21]. The uncertainty in the computed ingestion flow rates using the thermal model due to the reported 20% pressure measurement uncertainty is captured by the line thickness.

As shown in Fig. 7, the average percent difference between the empirical measurements and the predictions of the background flow model is 9% as the number of active pumps is increased from two to seven. By comparison, the change in ingestion flow rate predicted by the thermal model is 14–17 times smaller than the empirical measurements, resulting in an average percent difference of 93%.

The accuracy of the background flow model in predicting the empirical data is comparable to that of the current increment technique originally proposed by Walker and Gallimore [21]. In this technique, empirically measured changes in discharge current as a function of pressure are used in order to approximate the neutral ingestion flow rate [21]. However, application of this technique requires measurements of the operating characteristics of a given thruster across a range of facility backpressures. The comparable accuracy of the predictions of the background flow model to this empirical technique suggests that the model may be implemented in order to obtain these estimates of neutral ingestion without needing to perform the empirical mapping. Thus, taken together with the previously presented comparisons to the work of Hofer et al. [8], these results indicate that the background flow model is able to accurately replicate the empirically observed neutral ingestion characteristics of the P5 in the LVTF and offers a 60 to 70% improvement in accuracy over the thermal model [8].

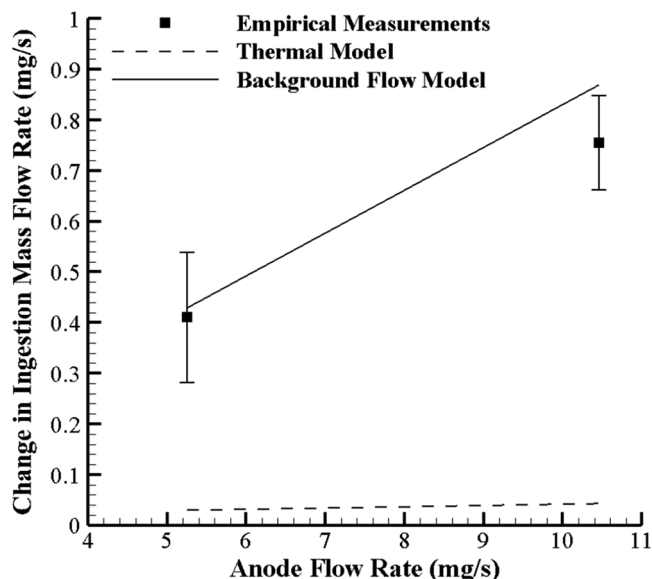


Fig. 7 Change in P5 ingestion flow rate between two and seven cryopumps.

B. H6 in the LVTF

The background flow model was developed without any considerations of HET-specific characteristics. As such, the model should be able to maintain the previously observed accuracy when predicting the ingestion characteristics of another thruster in the same facility. To evaluate this assertion, the predictions of the background flow model were compared to another dataset collected by Reid using the H6 HET in the LVTF [14,15]. The H6 is a 6 kW laboratory-model HET developed by the AFRL in collaboration with the NASA Jet Propulsion Laboratory and the University of Michigan [42]. In this work, Reid held the anode mass flow rate supplied to the H6 constant and the resultant discharge current was measured as the pressure in the LVTF was varied using a bleed flow of propellant [14,15]. As was the case with the P5, higher discharge currents were observed at higher facility pressures and attributed to an increase in neutral ingestion [14,15]. The observed change in discharge current can be used to estimate the concomitant change in effective anode flow rate using the method described previously.

The background flow model was similarly used to compute the ingestion flow rate for the H6 in the LVTF as a function of bleed flow rate for a discharge voltage of 300 V. The results are shown as a function of the bleed flow rate along with the empirical results in Fig. 8. The changes in ingestion flow rate predicted by the thermal model are also shown in Fig. 8. Consistent with the approach taken by Reid, the number densities used for the thermal model correspond to the average values acquired by a pair of ion gauges located on opposite walls at an axial distance equal to half the length of the LVTF [14,15]. Data presented by Reid show that the pressures reported at these two locations in the LVTF varied by an average of 70%; the error bars shown for the thermal model predictions correspond to the uncertainty in the thermal model computations associated with this variance in the pressure measurements [14]. The error bars shown for the empirical data in the figure correspond to the reported uncertainty in the measurements [14,15]. The results are reported as the change in ingestion flow rate relative to the baseline value obtained for an operating pressure of 1.9×10^{-5} Torr of Xe, which corresponds to a bleed flow of approximately 12 mg/s. It is important to note that, during the experiment, the bleed flow orifice was located beneath the thruster and oriented such that the flow of propellant impacted the underside of the thrust stand mounting structure [14]. Due to the one-dimensional nature of the background flow model, the radial injection of propellant could not be directly modeled. Instead, the bleed flow was approximated as another source entering the chamber as per the assumption regarding plume flow reflection in Sec. II.B.1.

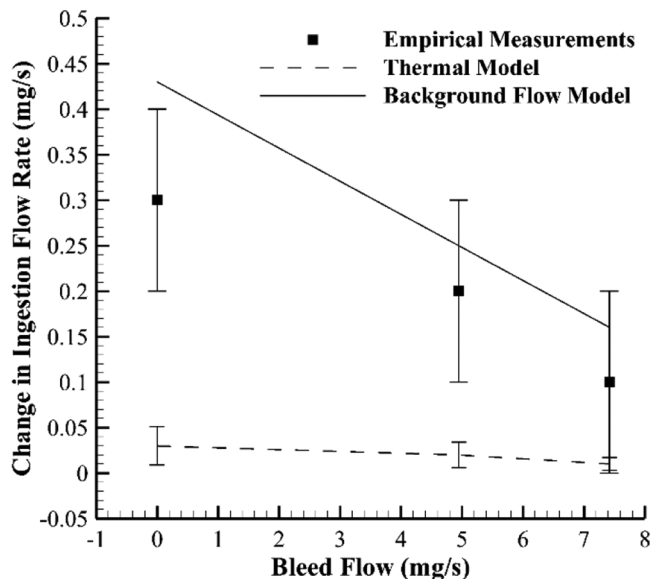


Fig. 8 Change in H6 ingestion mass flow rate with bleed flow in the LVTF.

As shown in Fig. 8, the values predicted by the thermal flow model are, on average, 10 times smaller than the empirical results. Even if the empirical measurements are all assumed to be equal to the lower uncertainty bound, the average percent difference between the predictions of the thermal model and the empirical results is 55%. However, the values predicted by the background flow model are of the same order as the empirical measurements and are within the uncertainty of the empirical measurements for the measurements taken at bleed flow rates of approximately 7.5 and 5 mg/s. For the final measurement, the predictions of the background flow model are only 8% different from the upper uncertainty bound. Thus, the predictions of the background flow model are approximately 50% closer to the empirical measurements than those generated using the thermal model. These results are identical to those for the 400 V operating condition also presented in the work by Reid [14,15].

The accuracy of the background flow model in predicting the empirical data is comparable to that of the empirically derived technique originally proposed by Reid [14,15]. In this technique, the effective ingestion area is assumed to be a hemisphere equal in diameter to the thruster outer diameter; all neutrals that cross this surface are assumed to undergo the same ionization process as the neutrals supplied to the anode [14,15]. However, as noted previously, this assumption has been disputed by other researchers [6]. The comparable accuracy of the predictions of the background flow model to this empirical technique suggests that the background flow model may be implemented in order to obtain estimates of the neutral ingestion mass flow rate without needing to make any assumption about ionization in the HET near-field plume. Taken together with the previously presented comparisons to the P5 in the LVTF, these results indicate that the background flow model is able to accurately replicate the empirically observed neutral ingestion characteristics of two different thrusters in the LVTF and offers a significant improvement in accuracy over the thermal model.

C. SPT-100 in Aerospace Corporation Facility

To assess the ability of the model to accurately predict trends in different facility types, a final dataset collected by Diamant et al. using the SPT-100 HET in the vacuum facility at The Aerospace Corporation was used for model validation [6]. The SPT-100 is a flight-model HET developed and built by the Fakel Experimental and Design Bureau with a nominal operating power of 1.35 kW [6]. The Aerospace Corporation's vacuum facility is a stainless-steel vacuum chamber measuring 9.8 m in length and 2.4 m in diameter, and it is equipped with 10 total cryosurfaces [6]. There are four cryopumps in the downstream pump region, four 1.2-m-diameter cryotubs in the upstream pump region, and two cryopumps on the upstream end dome [6]. Because the cryopumps used in The Aerospace Corporation's facility are the same model as those used in the LVTF, all of these cryosurfaces are assumed to be similar in terms of sticking coefficient and surface temperature to the cryopumps used in the LVTF.

In this work, the anode mass flow rate supplied to the SPT-100 was varied in order to maintain a constant discharge current as the vacuum facility pressure was varied via a combination of bleed mass flow addition and changing the number of active cryopumps [6]. As with the P5 and H6, the authors noted that higher anode flow rates were required to achieve a given discharge current at lower facility pressures and attributed the resultant change in anode flow rate to a decrease in neutral ingestion [6]. Using these data, the authors estimated the difference in flow rate between operation at the lowest achievable facility pressure (as measured by an ion gauge internally mounted adjacent to the HET) and vacuum conditions. Based on this estimate, the authors predicted a total ingestion flow rate of 0.03 mg/s. The background flow model was similarly used to compute the ingestion flow rate for the SPT-100 in The Aerospace Corporation's facility with all pumps on and no bleed flow. The background flow model predicted an ingested flow rate of approximately 0.02 mg/s, whereas the thermal model predicted an ingestion flow rate of 0.008 mg/s. The predictions of the background flow model were thus 40% closer to the empirical results than those of the thermal model and were computed without needing to obtain any empirical pressure measurements.

Although the aforementioned dataset will be explored in more detail in a later section, these initial results as well as those for the P5 and H6 indicate that the background flow model is significantly more accurate than the thermal model in predicting the ingestion characteristics of several different thrusters tested in different facilities with different pressure modulation techniques. It is important to note, however, that existing empirical evidence suggests that the modeled additional ingestion flow caused by bulk background flows is likely one of the contributors to the observed enhanced sensitivity of HETs to facility pressure beyond what would be predicted by the thermal model. Previous work has suggested that factors including spatial shifts in near-field plasma properties and the concomitant effects on electron transport can also contribute to HET operational changes as a function of facility pressure [9]. Nevertheless, the ability of the background flow model to obtain the predictions detailed in this section without empirical measurements, as well as the accuracy of the model across the described range of thruster and facility characteristics, has not, to the authors' knowledge, previously been demonstrated with any other mass ingestion or HET facility effects model, and therefore lends credibility to the background flow modeling approach [5–21].

IV. Model Studies

The background flow model is validated against several empirical datasets. In this section, the model is used to explore how parameters that often vary between different HET test facilities or test campaigns affect the neutral particle ingestion flow rates experienced by the HET being tested.

A. Pump Placement

The first model parameter to be evaluated will be pump placement within the test facility. As noted previously, facilities used for HET testing come in a wide variety of geometries and sizes [4]. These differences in geometric properties result in variations between facilities in the pump placement relative to the HET. Evidence of this can be seen from the preceding descriptions of the LVTF (in which all pumps are located upstream of the HET test station) and The Aerospace Corporation's facility (in which the pumps are distributed upstream and downstream of the HET test station, as well as on the upstream end dome) [6,21]. Current HET testing standards provide guidance regarding minimum facility pumping speeds and pressure measurement locations, but they often do not mention how pump placement within the facility can impact the background neutral flow environment or the operation of the HET itself [4,27].

To determine the impact of pump placement on the neutral ingestion characteristics of a HET, the background flow model was used to compare the ingestion flow rates of a given HET in a given facility as the pump locations were varied. Specifically, the ingestion flow rate of the P5 in the LVTF was computed for an anode flow rate of 15 mg/s and a discharge voltage of 300 V as the number of active cryopumps was increased from 2 to 12. These calculations were repeated for five different common pump geometries: upstream pumps only, downstream pumps only, distributed pumps with a 50/50% upstream/downstream pump split, distributed pumps with a 40/60% upstream/downstream pump split, and distributed pumps with a 20/20/60% end dome/upstream/downstream pump split. For convenience, hereafter, the upstream/downstream splits will be shown without the percent signs. The results comparing the first three configurations are shown in Fig. 9a, whereas the results comparing the different distributed pump distributions are shown in Fig. 9b.

As shown in Fig. 9a, the facility configuration with downstream pumps only has the lowest ingestion flow rate for all values of active cryopumps. As compared to the downstream pump-only configuration, the ingestion mass flow rate is between 3 and 21% higher if the only cryopumps are located upstream of the thruster with a mean percent difference of $12 \pm 7\%$ across all values of active cryopumps. The reported uncertainty represents one standard deviation of the dataset. Similarly, the ingested flow rate is between 2 and 15% higher for the distributed pump configuration with a 50/50 upstream/downstream pump split as compared to the configuration with downstream pumps with only a mean value of $9 \pm 5\%$.

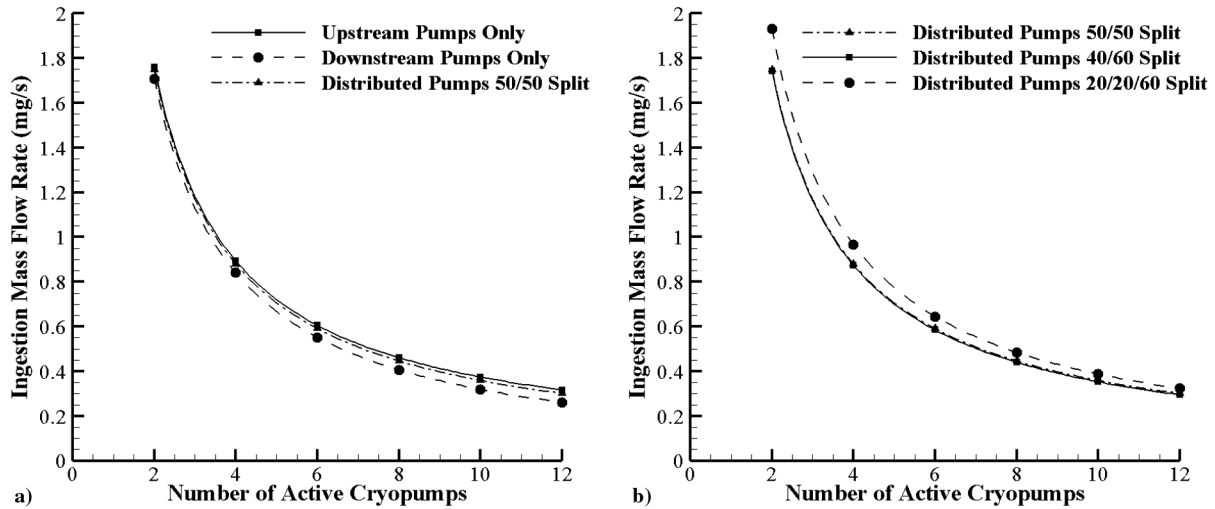


Fig. 9 Ingestion flow rate comparing a) upstream, downstream, and distributed pumps; and b) different distributed pump configurations.

As shown in Fig. 9b, the distributed pump configuration with the lowest ingestion flow rate is that with a 40/60 upstream/downstream pump split. As compared to the downstream pump-only configuration shown in Fig. 9a, the distributed pump configuration with a 40/60 upstream/downstream pump split has a 2 to 13% higher ingestion flow rate with a mean of $7 \pm 4\%$ across all values of active cryopumps. The distributed pump configuration with a 20/20/60 end dome/upstream/downstream pump split is the worst-performing pump configuration and has an ingestion flow rate that is 13–24% higher than the downstream pump-only configuration with a mean percent difference of $18 \pm 4\%$. Although the relative difference in ingestion flow rates between the different pump configurations is significant, overall, the ingestion flow rate for most values of active cryopumps represents less than 5% of the total mass flow rate supplied to the thruster (i.e., the sum of the anode flow rate and the ingestion flow rate). Thus, the overall deviation in total flow supplied to the HET is less than 1% between the configuration with the highest ingestion flow rates (i.e., the 20/20/60 end dome/upstream/downstream distributed pump split) and the one with the lowest ingestion flow rate (i.e., the downstream pumps only).

To understand why there is only a minimal difference in total flow supplied to the HET as a function of pump placement, the path an ingested neutral particle must take through the facility in order to be ingested by the HET must be discussed. As shown in Fig. 1b, the only neutrals that can be ingested by the HET are those that cross surface D traveling in the upstream direction. By assuming only 1-D motion, there are then only two paths that a given neutral can take in order to be ingested. The first (i.e., pathway 1) is where the neutral can reflect off the downstream pump surfaces and travel through the downstream region to the thruster exit plane without striking, and sticking to, a pump or being collisionally scattered by the HET plume. Neutrals that complete this transit must be on a trajectory to intersect the thruster exit plane in order to be ingested. Neutrals that follow a trajectory that lies outside of the thruster exit plane area have to follow a second pathway (i.e., pathway 2) in order to be ingested. These neutrals must travel through the upstream chamber region, reflect off the upstream chamber surfaces (and/or travel through the upstream end dome pump region), travel in the downstream direction back through the upstream and downstream pump regions, reflect off the downstream facility surfaces, and then travel back through the downstream pump region on a trajectory to intersect the thruster exit plane without being pumped or collisionally scattered in order to be ingested. Neutrals can repeat this second pathway as many times as needed until they are either pumped or ingested. Both pathways are illustrated in Fig. 10.

It is thus possible to define two components of the ingestion flow: one each contributed by the two pathways discussed previously. The magnitude of the first component (i.e., ingestion due to neutrals that traverse the downstream pump region on an intersecting trajectory

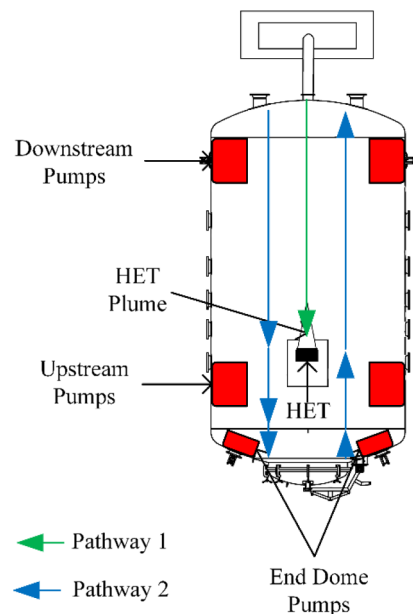


Fig. 10 Bulk background flow ingestion pathways.

with the HET exit plane) is inversely related to the pump surface area in the downstream pump region. Because, for a given number of pumps, the downstream-only pump configuration maximizes the downstream pump area, this component of the ingestion flow rate is thus minimized for this pump configuration. The magnitude of the second component (i.e., ingestion due to neutrals that have traversed the entire facility) is inversely related to the pump surface area in upstream and end dome pump regions. This component is thus maximized for the downstream-only pump configuration, but it is minimized for the other chamber configurations. As shown by the results in Fig. 9, these two competing effects largely offset each other and result in a minimal difference in ingestion flow rate as a function of pump configuration.

A similar analysis regarding the impact of pump placement on the background flowfield was conducted by Nakayama and Nakamura [24]. In that work, a two-dimensional DSMC code was used to assess the sensitivity of the background neutral pressure map to the pump location and facility aspect ratio. The model developed in this work is unable to provide similar guidance on the facility aspect ratio due to the assumption of one-dimensional motion. Furthermore, in the cited work, only the distance between the pumps and the HET was varied [24]. Despite these differences, both works suggest that maximization of the number of downstream pump surfaces

minimizes the number of background neutrals near the thruster exit plane, thus indicating good agreement between the more complex DSMC approach and the one-dimensional approach applied here [24].

B. Pressure Modulation Techniques

As shown by the empirical datasets referenced in Secs. III.A and III.B, existing empirical investigations into HET facility effects change the nominal operating pressure in the test facility by some combination of varying the gas load via the introduction of a bleed flow of propellant and modulating the effective pumping speed by changing the number of active cryopumps [43]. However, because the nominal operating pressure in a HET test facility can be expressed as the ratio of the gas load to the effective facility pumping speed, there are many combinations of bleed flow rate and pumping speed that can yield a given operating pressure [43]. To illustrate this, the pressure in the LVTF during P5 operation at an anode flow rate of 10.46 mg/s is computed as a function of the number of active cryopumps and the bleed flow rate of propellant. The results are shown in Fig. 11. For these computations, it is assumed that the gas load of the P5 is 1.25 Torr l/s and the nominal xenon pumping speed of the facility with all seven pumps on is 240,000 l/s. These numbers are consistent with values reported in previous investigations using the LVTF and are linearly scaled to account for the addition of bleed flow or the modulation of facility pumping speed [26]. Using this approach, the pressure P that would be measured by an ion gauge mounted on the wall of the LVTF near the exit plane of the HET can be computed as a function of the bleed flow rate of propellant \dot{m}_b and the number of active pumps n_p using Eq. (17):

$$P = \frac{1.25 \left(\frac{\dot{m}_b + 10.46}{10.46} \right)}{240,000 \left(\frac{n_p}{7} \right)} \quad (17)$$

Despite the fact that each of the surfaces shown in Fig. 11 yield the same facility operating pressure, previous work has shown that the method used to achieve this pressure (i.e., the combination of bleed flow and pumping speed) can impact the concomitant response of the HET [9,23]. To determine if HET neutral ingestion due to the bulk background flow is similarly affected by the method used to achieve a given facility pressure, the background flow model is used to compute the ingestion flow rate of neutrals into the P5 during operation at an anode flow rate of 10.46 mg/s in the LVTF for all combinations of bleed flow and pumping speed (i.e., number of active cryopumps), yielding a facility operating pressure of 2×10^{-5} Torr of Xe. The results are shown in Fig. 12. As done previously in the comparisons to empirical work with the H6, the bleed flow is approximated as another source entering the chamber, as per the assumption regarding plume flow reflection in Sec. II.B.1.

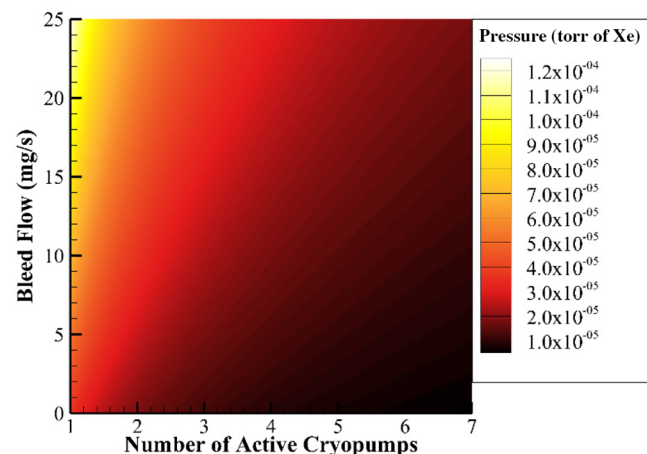


Fig. 11 LVTF operating pressure during P5 operation at an anode flow rate of 10.46 mg/s as a function of active pump quantity and bleed flow.

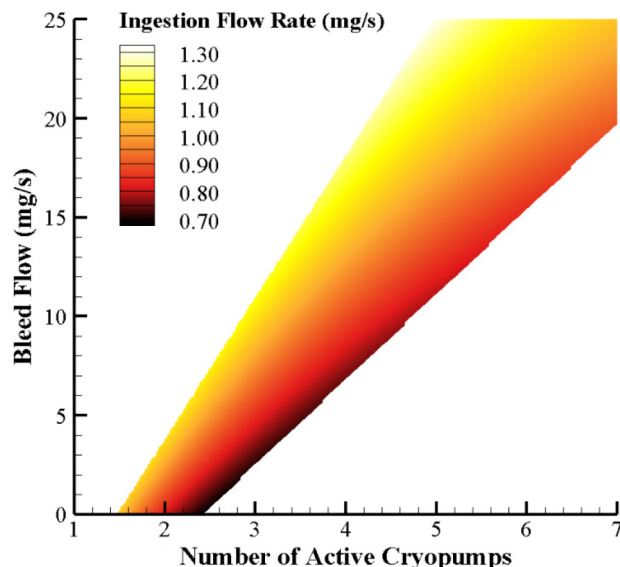


Fig. 12 Computed ingestion mass flow rates for P5 operation at an anode flow rate of 10.46 mg/s in the LVTF at a pressure of 2×10^{-5} Torr of Xe.

As shown in Fig. 12, at a fixed facility pressure of 2×10^{-5} Torr of Xe, the ingestion flow rate is not constant and varies, depending on the combination of bleed flow and pumping speed used to achieve that pressure. Specifically, the ingestion flow rate varies from a minimum value of 0.69 mg/s (7% of the anode flow rate) to a maximum value of 1.31 mg/s (12.5% of the anode flow rate). The percent difference between these maximum and minimum possible ingestion flow rates is thus 91%. These changes in ingestion flow rate furthermore result in up to a 5.6% variation in total flow rate (i.e., the sum of the constant anode flow rate and ingestion flow rate) supplied to the HET. This variation is larger than the approximately 2% variation seen by Hofer et al. in [8] for the P5 in the LVTF when the facility pumping speed was halved and was achieved without changing the facility operating pressure. These results are furthermore consistent with previous works, which have shown that the background neutral distribution within the test facility and the HET ingestion characteristics vary, depending on the method used to modulate the facility pressure [9,23]. Overall, these results indicate that pressure magnitude is not a sufficient parameter in order to understand and predict neutral ingestion by a HET and that significant variation in total flow rate (or, equivalently, discharge current) could be observed at a fixed facility pressure, depending on how that pressure is achieved.

It is important to note that, in practice, many researchers orient bleed flows such that they are injected radially or in the cross-stream direction relative to the HET plume [6,14]. Because of the one-dimensional nature of the background flow model, this radial motion cannot directly be captured, and all bleed flow is assumed to enter the facility traveling axially. This could cause the impact of bleed flow on ingestion flow rate to be overstated in the background flow model computations. To account for this, the ingestion flow rate was again computed by assuming that only one-quarter of the bleed flow was travelling axially in the facility. This reduction in number density corresponds to assuming that the bleed flow motion is two-dimensional (i.e., can travel in the axial and radial directions) and that the bleed flow has an equal probability of traveling in any of these directions. Even with this reduction to account for the radial motion of the bleed flow, the results of the background flow model indicate up to a 4% variation in total flow rate supplied to the HET at a facility operating pressure of 2×10^{-5} Torr of Xe, depending on how that pressure was achieved. This is still greater than the variation previously observed when the pumping speed in the LVTF was halved [8]. Furthermore, this variation is observed at a pressure below the thresholds recommended Dankanich et al. [27].

C. SPT-100 Performance Variation

To further explore how pressure modulation techniques may impact HET neutral ingestion, the thrust data collected by Diamant et al. for the SPT-100 HET in the vacuum facility at The Aerospace Corporation as a function of facility backpressure were revisited [6]. The measurements in this work indicated that the thrust of the SPT-100 decayed exponentially with decreasing facility pressure [6]. This trend was unlike the linear decay seen with other thrusters and facilities, and it was not accounted for by any existing model of neutral ingestion [5–21]. In this work, the facility pressure was varied via a combination of bleed flow and modulating the number of active pumps [6]. As shown previously, depending on how each pressure was achieved, this could result in a range of possible ingestion flow rates, and therefore a corresponding range of possible thrust values. If this range was large enough, it might have been able to capture the observed exponential trend for the SPT-100.

The background flow model was used to compute the ingestion flow rate of the SPT-100 HET in The Aerospace Corporation's facility for all combinations of bleed flow and pumping speeds yielding operating pressures between 1×10^{-5} Torr of Xe and 7×10^{-5} Torr of Xe (which matches the range over which empirical measurements were taken) [6]. To estimate the resultant impact of these ingestion flow rates on the performance of the SPT-100, the empirically estimated vacuum thrust value was linearly scaled by the ratio of the total flow rate supplied to the HET at a given pressure to that estimated for the zero backpressure case. This approach implicitly assumed that all ingested neutrals were ionized and accelerated identically to neutrals supplied via the thruster gas distributor and that the ingested neutrals did not change the ionization and acceleration processes within the HET. As noted previously, this simple ingestion approach was similar to that taken in many previous works on facility effects; furthermore, it was applied only to get a first-order estimate for the performance changes: these computations were not intended to fully predict the performance of the SPT-100 or capture all of the mode or operational changes that might be associated with neutral ingestion [8–10,14–16,21]. The results are shown in Fig. 13 along with the empirical trend line originally presented by Diamant et al. [6].

As noted previously and shown in Fig. 13, the range of potential ingestion mass flow rates at a given pressure results in a range of possible thrust values. Only thrust values corresponding to the maximum and minimum predicted ingestion flow rates at each pressure are shown. In other words, the points composing the maximum prediction line correspond to the predicted thrust values that would be measured for those facility conditions that yield the highest ingestion flow rate at each of the pressures shown on the abscissa, whereas the minimum prediction line contains the points

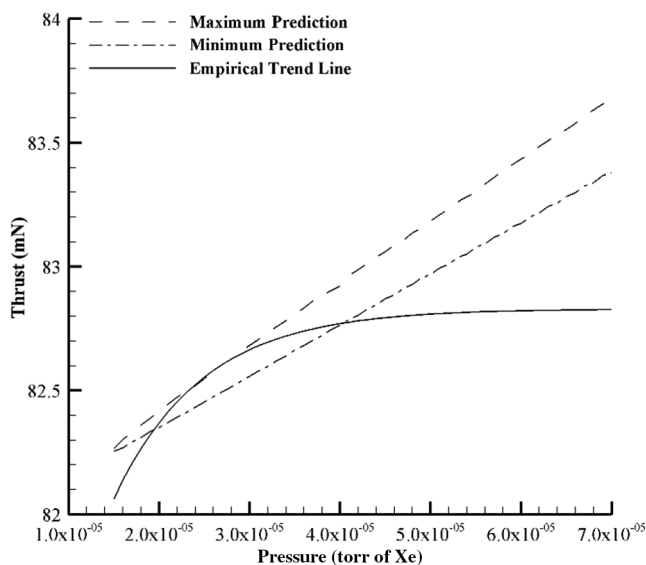


Fig. 13 Predicted and measured thrust of the SPT-100 HET as a function of The Aerospace Corporation's facility pressure.

corresponding to the predicted thrust values that would be measured for those facility conditions that yield the lowest ingestion flow rate at each pressure. Between these two lines is a range of points that represent all of the thrust values that could be measured at each pressure according to the background flow model.

As shown in Fig. 13, this range is large enough to encompass the exponential decay in thrust observed by Diamant et al. within the stated experimental uncertainty of approximately 0.5 mN [6]. These results therefore suggest that the observed exponential decay could have been the result of the pathway used to achieve each pressure and the resultant nonlinear impact on neutral ingestion by the HET. In other words, due to the size of the range of possible thrust values at each pressure, the background flow model suggests that it is possible to plot a pathway through this range that would yield an apparent exponential decay in thrust with facility pressure. To the authors' knowledge, this is the first analytical model to be able to offer insight into these observed trends [6]. It is important to note, that although the background flow model is consistent with the observed empirical trends, it is not able to replicate the observed asymptote at pressures above 5.0×10^{-6} Torr of Xe. It is likely this behavior is due to the other processes that have been observed to impact HET operation as a function of facility pressure, including spatial shifts in near-field plasma properties and the concomitant effects on electron transport that are not captured by the background flow model [9].

D. Parameter Sensitivities

As shown in Eqs. (14) and (15), the predicted ingestion flow rate computed by the background flow model is impacted directly by three parameters for which the values have been assumed: the chamber wall temperature, the pump surface temperature, and the pump sticking coefficient. Because these factors could vary between different facilities, the assumption of a uniform value for these three parameters may have introduced error in the estimates made by the background flow model. To quantify this potential error, the sensitivity of the predictions made by the background flow model to these parameters must be determined.

The first parameter sensitivity to be evaluated is that related to the facility wall temperature. This sensitivity is of particular importance because, in many HET test facilities, the plume is directed toward a graphite beam dump that is separate from the facility walls. As the beam dump is directly impinged upon by the plume, the beam dump surface temperature may be higher than the facility wall temperature; thus, the neutrals reflecting off this surface could have a velocity characterized by a higher temperature. For this sensitivity study, the background flow model is used to compute the ingestion flow rate for the P5 in the LVTF at the 10.46 mg/s operating condition as a function of chamber wall temperature, holding all other variables constant. The results are shown for three different types of pump configurations in Fig. 14a and indicate that the predicted ingestion flow rate varies by approximately 3.5% as the facility wall temperature is changed from 273 to 350 K for all pump configurations. In terms of the total flow rate supplied to the HET, the variation over that temperature range is less than 0.1%.

To determine the sensitivity of the background flow model to the assumed pump surface temperature, the background flow model was used to compute the ingestion flow rate of the P5 in the LVTF at the 10.46 mg/s operating condition as a function of pump surface temperature, holding all other variables constant. The results are shown for three different types of pump configurations in Fig. 14b and indicate that the predicted ingestion flow rate varies by less than 0.1% as the pump surface temperature is changed from 10 to 50 K for all pump configurations. The chosen temperature range encompasses all reported surface temperatures of cryosurfaces used to pump xenon during HET testing [22,44].

The final parameter to be evaluated is the pump sticking coefficient. For this sensitivity study, the background flow model is used to compute the ingestion flow rate of the P5 in the LVTF at the 10.46 mg/s operating condition as a function of the pump sticking coefficient, holding all other variables constant. The results are shown for three different types of pump configurations in Fig. 14c.

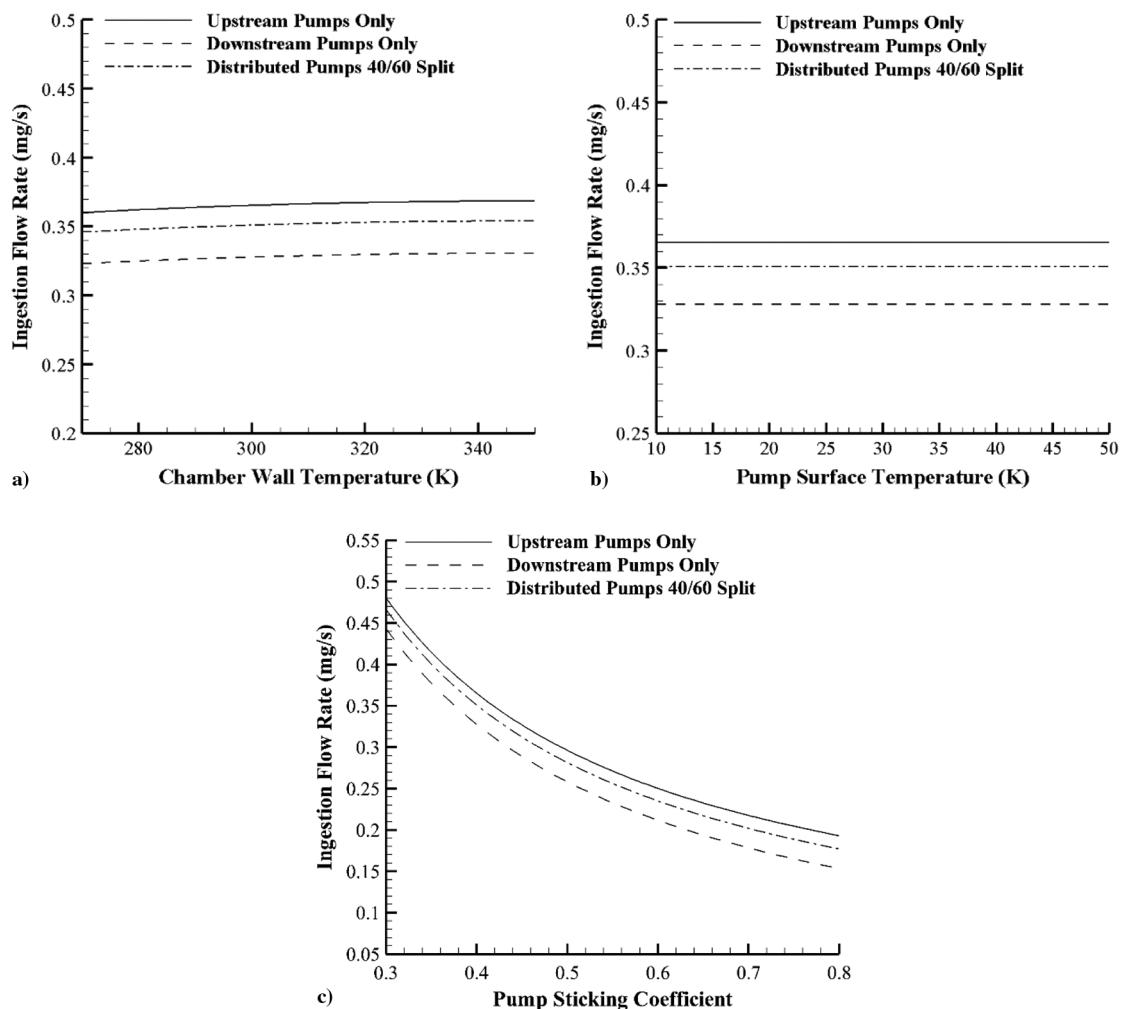


Fig. 14 Results sensitivity to a) chamber wall temperature, b) pump surface temperature, and c) pump sticking coefficient.

The observed sensitivity to the pump sticking coefficient is larger than that observed for either the chamber wall temperature or the pump surface temperature. As the pump sticking coefficient is changed from 0.3 to 0.8, the HET ingestion flow rate decreases by an average of 60% for all pump configurations.

This large variation is expected because the pump sticking coefficient determines the effectiveness with which the cryosurfaces remove xenon from the background flow environment, and thus can have similar influence to the addition of extra pumping surfaces. However, because the ingestion flow rate represents such a small fraction of total flow supplied to the HET, the variation in total flow is less than 3%. Furthermore, the assumed sticking coefficient of 0.4 is empirically determined for the LVTF using detailed maps of the neutral density inside of the facility during HET operation [22,26]. As the majority of the empirical results used for comparison are acquired in the LVTF, it is expected that the error associated with this choice of sticking coefficient is minimal. Therefore, overall, the background flow model shows minimal sensitivity to the assumed empirical parameters.

E. Discussion of the One-Dimensional Flow Assumption

Among the assumptions discussed in Sec. II.B.1, perhaps the most restrictive is the assumption of a one-dimensional background flow. Although consistent with the approach taken by Cai et al., it is nonetheless worthwhile to discuss the relevance of this assumption and resultant impacts on the model, as well as the results it generates [22,30,36]. The first implication of this assumption is that the background neutrals are constrained to move only in the axial direction. To assess the validity of this constraint, it is necessary to discuss the typical reflection geometry in HET ground test facilities.

In the facilities mentioned as part of this work, the HET plume flow is directed toward a carbon beam dump composed of several flat graphite panels [45]. As the HET plume is axially accelerated, the incident particles reflect off these flat surfaces with a bulk velocity that is primarily oriented in the axial direction, thus minimizing the error associated with the one-dimensional flow assumption for the facilities used in this work [46]. This rationale has been empirically supported by pressure measurements, which have found minimal bulk background gas entrainment into radially facing gauges but significant entrainment into gauges facing axially [23]. This suggests that the bulk flow of the background gas is primarily in the axial direction. The impact of nonflat plume reflection geometries on the validity of the one-dimensional flow assumption is not presently clear and will be explored in future work.

By assuming a one-dimensional flow, all collisions between the background neutrals and facility sidewalls are also neglected. These collisions modify the speed distribution of the background neutrals. As per the assumptions laid out in Sec. II.B.1, upon colliding with the facility sidewall, an incident neutral will thermalize, and thus be reflected with a speed characterized by the facility wall temperature. For incident particles with speeds characterized by another temperature (i.e., those at pump temperature), these collisions will then result in a change in velocity and a concomitant change in number density as per Eq. (5). To assess the error associated with neglecting this effect, the background flow model was used to compute the ingestion mass flow rate for the P5 HET operating in a facility with 10 pumps located downstream of the HET. The downstream pump-only configuration is selected because it maximizes the population of neutrals crossing surface D in the

upstream direction with a speed characterized by a temperature other than the facility wall temperature, thus representing the worst-case estimate of the error. The ingestion flow rate is then computed again, assuming all particles not at wall temperature undergo a sidewall collision before crossing surface D, which again represents the worst-case deviation from the model assumptions. The deviation between this result and the one computed neglecting the sidewall effects differs by less than 1%.

V. Conclusions

This work expanded the background flow model first proposed by Cai et al. and explored the applicability of this approach to modeling neutral ingestion by HETs [22]. The original model was further developed and generalized to describe the background flow environment in facilities with any combination of end dome, upstream, and downstream pumps; and analytic expressions were developed for the ingestion flow rate of a HET due to the background neutral flow within the facility. The predictions generated by these expressions were compared against empirical data taken with the P5, H6, and SPT-100 HETs in two different facilities and found to match the empirical observations to within the experimental uncertainty. These predictions were furthermore shown to be 40 to 70% more accurate than those generated using the thermal model most commonly used to predict and estimate neutral ingestion by HETs; and they were found equally as accurate as specific semiempirical models developed for the P5 and H6, without requiring any empirical inputs such as in situ pressure measurements [14,15,21]. The demonstrated improvement over the thermal model as well as the demonstrated accuracy in predicting empirical measurements for a variety of thrusters and facilities is, to the authors' knowledge, unique to the background flow model, thus lending credibility to this modeling approach and supporting its value as a predictive analytical tool [5–21].

The validated background flow model was used to assess the impact of parameters that often vary between different test facilities and test campaigns on HET neutral ingestion. It was shown that neutral ingestion could vary by as much as 24%, depending on where the pumps were placed within a test facility; the lowest ingestion flow rates occurred for facilities with the maximum number of pumps located downstream of the HET. The impact of pressure modulation techniques on HET neutral ingestion was also investigated, and it was shown that the ingestion flow rate of a HET could vary by as much as 91% at a fixed facility pressure of 2×10^{-5} Torr of Xe, depending on the combination of bleed flow and pumping speed used to achieve that pressure. This resulted in a band of possible ingestion flow rates and performance characteristics at a given pressure that was large enough to capture the empirically observed exponential decay of the thrust of the SPT-100 with decreasing facility pressure [6]. The sensitivity of these results to the assumed parameters of chamber wall temperature, pump surface temperature, and pump sticking coefficient were assessed and shown to be less than 3% of the predicated total HET flow. Overall, these results indicated that pressure magnitude is not a sufficient variable for quantifying neutral ingestion by a HET, and that other test variables (i.e., pressure modulation technique) must be specified and held constant in order to fully describe HET ingestion characteristics.

References

- [1] Brophy, J. R., Friedman, L., and Culik, F., "Asteroid Retrieval Feasibility," *2012 IEEE Aerospace Conference*, IEEE, Piscataway, NJ, 2012, pp. 1–16.
doi:10.1109/AERO.2012.6187031
- [2] Brophy, J. R., "Advanced Solar Electric Propulsion for Planetary Defense and Asteroid Resource Utilization," *34th International Electric Propulsion Conference*, Electric Rocket Propulsion Society, IEPC Paper 2015-065, Fairview Park, OH, 2015.
- [3] Marchandise, F. R., and Koppel, C. R., "Electric Propulsion for Deep Space: A Study Case «Jupiter ICy Moon» with EP," *34th International Electric Propulsion Conference*, Electric Rocket Propulsion Society, IEPC Paper 2015-065, Fairview Park, OH, 2015.
- [4] Semenko, A., Kim, V., Gorshkov, O., and Jankovsky, R., "Development of Electric Propulsion Standards-Current Status and Further Activity," *27th International Electric Propulsion Conference*, Electric Rocket Propulsion Society, IEPC Paper 2001-070, Fairview Park, OH, 2001.
- [5] Brown, D. L., and Gallimore, A. D., "Evaluation of Plume Divergence and Facility Effects on Far-Field Faraday Probe Current Density Profiles," *31st International Electric Propulsion Conference*, Electric Rocket Propulsion Society, IEPC Paper 2009-030, Fairview Park, OH, 2009.
- [6] Diamant, K. D., Liang, R., and Corey, R. L., "The Effect of Background Pressure on SPT-100 Hall Thruster Performance," *50th AIAA/ASME/SAE/ASEE Joint Propulsion Conference and Exhibit*, AIAA Paper 2014-3710, 2014.
doi:10.2514/6.2014-3710
- [7] Goebel, D. M., and Katz, I., *Fundamentals of Electric Propulsion: Ion and Hall Thrusters*, Wiley, Hoboken, NJ, 2008, pp. 32–34, 325–384, 463–467.
- [8] Hofer, R. R., Peterson, P. Y., and Gallimore, A. D., "Characterizing Vacuum Facility Backpressure Effects on the Performance of a Hall Thruster," *27th International Electric Propulsion Conference*, Electric Rocket Propulsion Society, IEPC Paper 2001-045, Fairview Park, OH, 2001.
- [9] Hofer, R. R., and Anderson, J. R., "Finite Pressure Effects in Magnetically Shielded Hall Thrusters," *50th AIAA/ASME/SAE/ASEE Joint Propulsion Conference and Exhibit*, AIAA Paper 2014-3709, 2014.
doi:10.2514/6.2014-3709
- [10] Huang, W., Kamhawi, H., Lobbia, R. B., and Brown, D. L., "Effect of Background Pressure on the Plasma Oscillation Characteristics of the HiVHAc Hall Thruster," *50th AIAA/ASME/SAE/ASEE Joint Propulsion Conference and Exhibit*, AIAA Paper 2014-3708, 2014.
doi:10.2514/6.2014-3708
- [11] Kamhawi, H., Huang, W., Haag, T., and Spektor, R., "Investigation of the Effects of Facility Background Pressure on the Performance and Voltage-Current Characteristics of the High Voltage Hall Accelerator," *50th AIAA/ASME/SAE/ASEE Joint Propulsion Conference and Exhibit*, AIAA Paper 2014-3707, 2014.
doi:10.2514/6.2014-3707
- [12] Nakles, M. R., and Hargus, W. A., "Background Pressure Effects on Ion Velocity Distribution Within a Medium-Power Hall Thruster," *Journal of Propulsion and Power*, Vol. 27, No. 4, 2011, pp. 737–743.
doi:10.2514/1.48027
- [13] Randolph, T., Kim, V., Kaufman, H. R., Kozubsky, K., Zhurin, V. V., and Day, M., "Facility Effects on Stationary Plasma Thruster Testing," *23rd International Electric Propulsion Conference*, Electric Rocket Propulsion Society, IEPC Paper 1993-093, Fairview Park, OH, 1993.
- [14] Reid, B. M., "The Influence of Neutral Flow Rate in the Operation of Hall Thrusters," Ph.D. Dissertation, Aerospace Engineering Dept., Univ. of Michigan, Ann Arbor, MI, 2009, pp. 306–319.
- [15] Reid, B. M., "Empirically-Derived Corrections for Facility Effects in Performance and Plume Measurements of Hall Thrusters," *34th International Electric Propulsion Conference*, Electric Rocket Propulsion Society, IEPC Paper 2015-362, Fairview Park, OH, 2015.
- [16] Tighe, W. G., Spektor, R., Diamant, K., and Kamhawi, H., "Effects of Background Pressure on the NASA 173M Hall Current Thruster Performance," *34th International Electric Propulsion Conference*, Electric Rocket Propulsion Society, IEPC Paper 2015-152, Fairview Park, OH, 2015.
- [17] Byers, D., and Dankanich, J., "A Review of Facility Effects on Hall Effect Thrusters," *31st International Electric Propulsion Conference*, Electric Rocket Propulsion Society, IEPC Paper 2009-076, Fairview Park, OH, 2009.
- [18] Crofton, M. W., and Pollard, J., "Thrust Augmentation by Charge Exchange," *49th AIAA/ASME/SAE/ASEE Joint Propulsion Conference and Exhibit*, AIAA Paper 2013-4131, 2013.
doi:10.2514/6.2013-4131
- [19] Diamant, K., Spektor, R., Beiting, E., Young, J., Curtiss, T., and Corporation, T. A., "The Effects of Background Pressure on Hall Thruster Operation," *48th AIAA/ASME/SAE/ASEE Joint Propulsion Conference and Exhibit*, AIAA Paper 2012-3735, 2012.
doi:10.2514/6.2012-3735
- [20] Huang, W., Kamhawi, H., and Haag, T., "Effect of Background Pressure on the Performance and Plume of the HiVHAc Hall Thruster," *33rd International Electric Propulsion Conference*, Electric Rocket Propulsion Society, IEPC Paper 2013-058, Fairview Park, OH, 2013.
- [21] Walker, M. L. R., and Gallimore, A. D., "Performance Characteristics of a Cluster of 5-kW Laboratory Hall Thrusters," *Journal of Propulsion and Power*, Vol. 23, No. 1, 2007, pp. 35–43.
doi:10.2514/1.19752

- [22] Cai, C., Boyd, I. D., and Sun, Q., "Free Molecular Background Flow in a Vacuum Chamber Equipped with Two-Sided Pumps," *Journal of Vacuum Science and Technology A: Vacuum, Surfaces, and Films*, Vol. 24, No. 1, 2006, pp. 9–19.
doi:10.1116/1.2126678
- [23] Yim, J., and Burt, J. M., "Characterization of Vacuum Facility Background Gas Through Simulation and Considerations for Electric Propulsion Ground Testing," *51st AIAA/SAE/ASEE Joint Propulsion Conference*, AIAA Paper 2015-3825, 2015.
doi:10.2514/6.2015-3825
- [24] Nakayama, Y., and Nakamura, M., "Electric Propulsion Propellant Flow within Vacuum Chamber," *34th International Electric Propulsion Conference*, Electric Rocket Propulsion Society, IEPC Paper 2015-360, Fairview Park, OH, 2015.
- [25] Frieman, J. D., King, S. T., Walker, M. L., and Khayms, V., "Preliminary Assessment of the Role of a Conducting Vacuum Chamber in the Hall Effect Thruster Electrical Circuit," *50th AIAA/ASME/SAE/ASEE Joint Propulsion Conference and Exhibit*, AIAA Paper 2014-3712, 2014.
doi:10.2514/6.2014-3712
- [26] Walker, M. L. R., "Effects of Facility Backpressure on the Performance and Plume of a Hall Thruster," Ph.D. Dissertation, Aerospace Engineering Dept., Univ. of Michigan, Ann Arbor, MI, 2005, pp. 111–155.
- [27] Dankanich, J., Walker, M. L. R., Swiatek, M., and Yim, J., "Recommended Practice for Pressure Measurements and Calculation of Effective Pumping Speeds During Electric Propulsion Testing," *33rd International Electric Propulsion Conference*, Electric Rocket Propulsion Society, IEPC Paper 2013-358, Fairview Park, OH, 2013.
- [28] Frieman, J. D., King, S. T., Walker, M. L. R., Khayms, V., and King, D., "Role of a Conducting Vacuum Chamber in the Hall Effect Thruster Electrical Circuit," *Journal of Propulsion and Power*, Vol. 30, No. 6, 2014, pp. 1471–1479.
doi:10.2514/1.B35308
- [29] Anderson, J. D., *Fundamentals of Aerodynamics*, McGraw-Hill Education, New York, 2010, pp. 54–57.
- [30] Cai, C., "Theoretical and Numerical Studies of Plume Flows in Vacuum Chambers," Ph.D. Dissertation, Aerospace Engineering Dept., Univ. of Michigan, Ann Arbor, MI, 2005, pp. 22–76.
- [31] Choueiri, E. Y., "Plasma Oscillations in Hall Thrusters," *Physics of Plasmas*, Vol. 8, No. 4, 2001, pp. 1411–1426.
doi:10.1063/1.1354644
- [32] Ketsdever, A. D., "Design Considerations for Cryogenic Pumping Arrays in Spacecraft–Thruster Interaction Facilities," *Journal of Spacecraft and Rockets*, Vol. 38, No. 3, 2001, pp. 400–410.
doi:10.2514/2.3698
- [33] Cedolin, R. J., Hargus, W. A., Storm, P. V., Hanson, R. K., and Cappelli, M. A., "Laser-Induced Fluorescence Study of a Xenon Hall Thruster," *Applied Physics B: Lasers and Optics*, Vol. 65, No. 4, 1997, pp. 459–469.
doi:10.1007/s003400050297
- [34] Boyd, I. D., "A Review of Hall Thruster Plume Modeling," *38th Aerospace Sciences Meeting and Exhibit*, AIAA Paper 2000-0466, 2000.
doi:10.2514/6.2000-466
- [35] Walker, M. L. R., and Gallimore, A. D., "Neutral Density Map of Hall Thruster Plume Expansion in a Vacuum Chamber," *Review of Scientific Instruments*, Vol. 76, No. 5, 2005, Paper 053509.
doi:10.1063/1.1915011
- [36] Cai, C., Boyd, I., and Sun, Q., "Rarefied Background Flow in a Vacuum Chamber Equipped with One-Sided Pumps," *Journal of Thermophysics and Heat Transfer*, Vol. 20, No. 3, July 2006, pp. 524–535.
doi:10.2514/1.19178
- [37] Walker, M., Gallimore, A., Cai, C., and Boyd, I., "Pressure Map of a Facility as a Function of Flow Rate to Study Facility Effects," *38th AIAA/ASME/SAE/ASEE Joint Propulsion Conference and Exhibit*, AIAA Paper 2002-3815, 2002.
doi:10.2514/6.2002-3815
- [38] Martinez, R., Dao, H., Walker, M., and Tech, G., "Power Deposition into the Discharge Channel of a Hall Effect Thruster," *Journal of Propulsion and Power*, Vol. 30, No. 1, Jan. 2014, pp. 209–220.
doi:10.2514/1.B34897
- [39] Boyd, I. D., and Dressler, R. A., "Far Field Modeling of the Plasma Plume of a Hall thruster," *Journal of Applied Physics*, Vol. 92, No. 4, 2002, pp. 1764–1774.
doi:10.1063/1.1492014
- [40] Reid, B. M., and Gallimore, A. D., "Review of Hall Thruster Neutral Flow Dynamics," *30th International Electric Propulsion Conference*, Electric Rocket Propulsion Society, IEPC Paper 2007-038, Fairview Park, OH, 2007.
- [41] Hofer, R., "Development and Characterization of High-Efficiency, High-Specific Impulse Xenon Hall Thrusters," Ph.D. Dissertation, Aerospace Engineering Dept., Univ. of Michigan, Ann Arbor, MI, 2004, pp. 67–69.
- [42] Sekerak, M. J., "Plasma Oscillations and Operation Modes in Hall Effect Thrusters," Ph.D. Dissertation, Aerospace Engineering Dept., Univ. of Michigan, Ann Arbor, MI, 2014, pp. 55–58.
- [43] Dushman, S., and Lafferty, J. M., *Scientific Foundations of Vacuum Technique*, Wiley, New York, 1962, pp. 347–374.
- [44] Garner, C., Polk, J., Brophy, J., and Goodfellow, K., "Methods for Cryopumping Xenon," *32nd Joint Propulsion Conference and Exhibit*, AIAA Paper 1996-3206, 1996.
doi:10.2514/6.1996-3206
- [45] Huang, W., Gallimore, A. D., and Hofer, R. R., "Neutral Flow Evolution in a Six-Kilowatt Hall Thruster," *Journal of Propulsion and Power*, Vol. 27, No. 3, May 2011, pp. 553–563.
doi:10.2514/1.B34048
- [46] Pollard, J. E., and Beiting, E. J., "Ion Energy, Ion Velocity, and Thrust Vector Measurements for the SPT-140 Hall Thruster," *Proceedings of the 3rd International Conference on Spacecraft Propulsion*, 3AF: Assoc. Aéronautique Astronautique de France, Paris, 2000, pp. 789–796.

J. Blandino
Associate Editor